IEEE Photonics Journal
An IEEE Photonics Society Publication

Add/Drop Mode-Division Multiplexer Based on a Mach–Zehnder Interferometer and Periodic Waveguides

Volume 7, Number 4, August 2015

D. Pérez-Galacho
D. Marris-Morini
A. Ortega-Moñux
J. G. Wangüemert-Pérez
L. Vivien

DOI: 10.1109/JPHOT.2015.2446765
1943-0655 © 2015 IEEE

Add/Drop Mode-Division Multiplexer Based on a Mach–Zehnder Interferometer and Periodic Waveguides

D. Pérez-Galacho,[1] D. Marris-Morini,[1] A. Ortega-Moñux,[2] J. G. Wangüemert-Pérez,[2] and L. Vivien[1]

[1]Institut d'Electronique Fondamentale, Université Paris-Sud, CNRS UMR 8622, 91405 Orsay, France
[2]Departamento de Ingeniería de Comunicaciones, ETSI Telecomunicación, Universidad de Málaga, 29010 Málaga, Spain

DOI: 10.1109/JPHOT.2015.2446765

Manuscript received May 11, 2015; revised June 15, 2015; accepted June 15, 2015. Date of current version July 2, 2015. Corresponding author: D. Pérez-Galacho (e-mail: diego.perez-galacho@u-psud.fr).

Abstract: Mode-division multiplexing (MDM) is currently under study due to its potential to further increase data rates in optical communication circuits. In this paper, we propose an add/drop MDM for the first- and second-order modes that cover the whole C-Band (1.53–1.57 μm). The device is based on a Mach–Zehnder interferometer, including periodic waveguides in the arms. Mode selectivity is provided by means of the periodic waveguides, which are designed to allow the propagation of the second mode and to reflect the first mode. The proposed device exhibits less than 1 dB insertion loss and more than 30 dB extinction ratio in the whole C-Band. Furthermore, it presents wide fabrication tolerances.

Index Terms: Mode-division multiplexing, periodic waveguides, subwavelength grating, Bragg grating.

1. Introduction

Bandwidth demand in optical communication systems is continuously growing [1], [2]. Wavelength Division Multiplexing (WDM) circuits were proposed to increase the aggregate bandwidth of the optical communications. However, WDM is reaching its limits and to further increase the aggregate bandwidth another level of orthogonality is needed. Mode Division Multiplexing (MDM) appears as a solution to keep up with bandwidth requirement [3]. Even though it is possible to find nowadays good solutions for implementing MDM systems in fiber optics and in free space optics [4], [5], in planar integrated optics MDM systems are still in a early research stage. Several propositions of devices and subsystems for MDM in integrated optics appeared recently, including mode converters, combiners and add/drop multiplexers. These devices usually rely either on Y-junctions [6]–[8], which can require tight fabrication tolerances or on evanescent coupling by means of Directional Couplers (DC) [9]–[13], Tapered Directional Couplers (TDC) [14] or Ring Resonators (RR) [15], [16], which are intrinsically narrowband. In this work we present a novel kind of Add/Drop Mode Division Multiplexer that overcomes those constraints, it is based on a Mach–Zehnder interferometers with periodic waveguide grating as arms. The device exhibits Insertion Loss below 1 dB and Extinction Ratio higher than 30 dB for a bandwidth

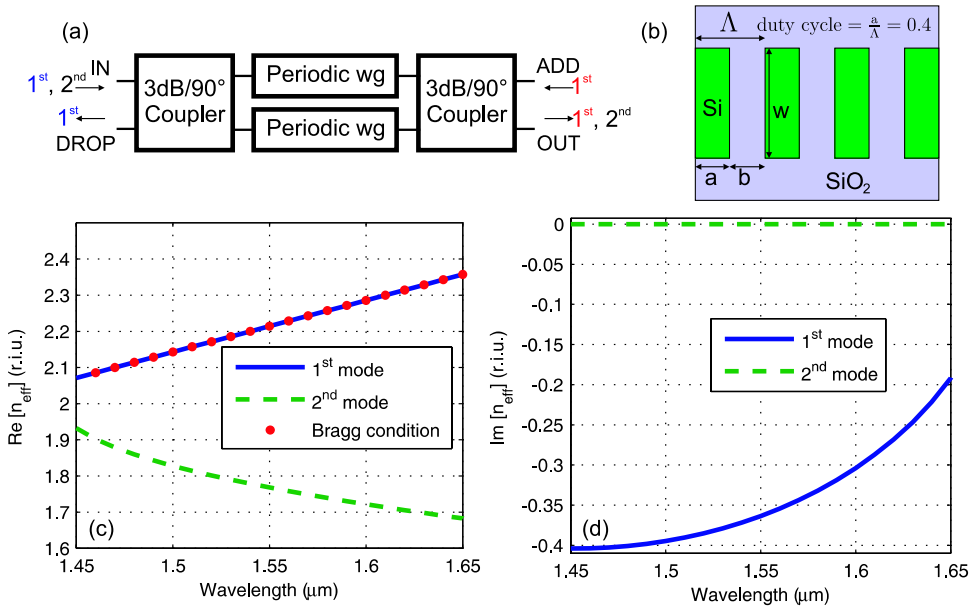

Fig. 1. Principle of operation of the proposed Add/Drop Mode Division Multiplexing. (a) Schematic view. (b) Detail of the periodic waveguide. (c) and (d) Real part and imaginary part of the Bloch modes effective indices.

exceeding the whole C-Band of optical communication (1.53–1.57 μm). Furthermore, it can be fabricated with standard Deep-UV lithography.

This paper is organized as follows. In Section 2, the principle of operation of the device and the physical phenomenon in which it is based are presented and discussed. Section 3 is devoted to the design of each part of the device. The simulation results of the complete device are presented in Section 4, along with an explanation on the simulation procedure and a study of tolerance to fabrication errors. Finally, Section 5 summarizes the main conclusions of this work.

2. Principle of Operation

The proposed device consists on a Mach–Zehnder interferometer including periodic waveguides in both arms [see Fig. 1(a)]. The principle of operation is the following: the first and second order modes go into the device through the port IN. Both modes are split by the first 3 dB/9° coupler. In the periodic waveguides the first order mode is reflected and then combined into the 3 dB/90° coupler in the DROP port, whereas the second order mode is propagated through the periodic waveguide grating and is combined by the 3 dB/90° coupler in the OUT port. Another first order mode can also be introduced in the ADD port to be coupled with the second order mode in the OUT port. The ability of a periodic waveguide grating to allow the propagation of the second order mode whereas reflecting the first order mode is shown in Fig. 1(c) and (d), where the real and the imaginary part of the effective index of both first and second order Bloch modes of a periodic waveguide [see Fig. 1(b)] are represented. It can be clearly seen that the first mode is within the Bragg regime $(\mathrm{Re}[n_{\mathrm{eff}}] = \lambda/2\Lambda)$, i.e., being reflected, while the second mode is in the sub-wavelength regime and can propagate without losses or reflections in the periodic structure [17], [18]. Furthermore, Fig. 1(d) clearly shows how this phenomenon can be used to cover the whole C-Band (1.53–1.57 μm). The calculation is reported for a 300 nm height silicon on insulator (SOI) fully etched (strip) waveguides. The width (w) is 1 μm to ensure multimode operation. The pitch (Λ) is 350 nm, and the duty cycle is 0.4. It can be noticed that the same principle can be obtained with different waveguide dimensions, such as 220 nm height SOI for either strip or rib waveguides.

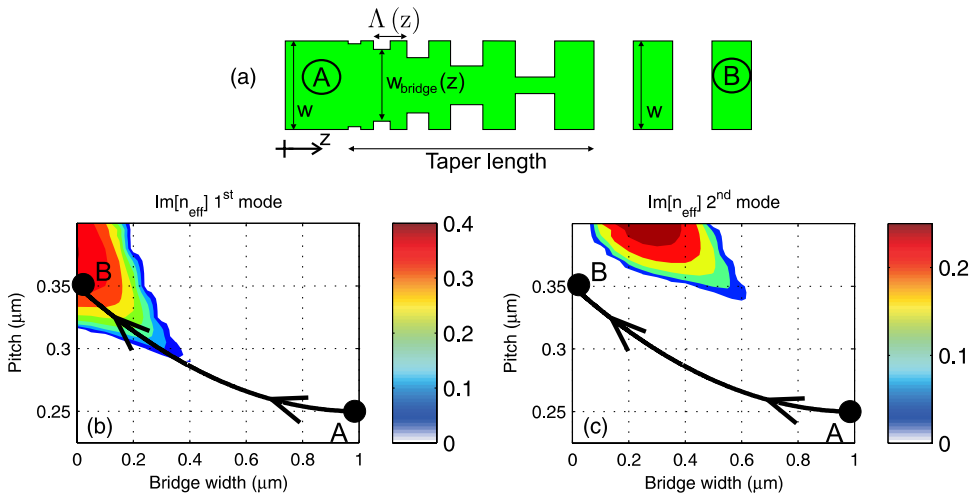

Fig. 2. Details on taper design procedure. (a) Schematic structure of the proposed taper. (b) and (c) Maps of the imaginary part of the Bloch effective index for the first- and second-order mode, respectively (Wavelength $= 1.55\ \mu$m).

3. Device Design

Once the periodic waveguide that provides the selectivity between the first- and second-order modes is designed, a transition (taper) between conventional strip waveguide and periodic waveguide has to be designed. The design of the tapers was based on the method proposed in [19], with some modifications for taking into account two modes instead of one. The structure of the proposed transition is sketched in Fig. 2(a). Two parameters (the bridge width (w_{bridge}) and pitch (Λ)) change along the taper length while the waveguide width (W) was kept constant. Imaginary part of the Bloch effective index as a function of bridge width and pitch for the first and second order modes are shown in Fig. 2(b) and (c), respectively. These maps were computed by means of a 2-D in-house simulation tool (FEXEN) specifically designed for Bloch mode calculations [20]. Colored regions, where the imaginary part of the reflective index is different from zero correspond to the Bragg regime for each mode. The tapers have to be designed so that the second mode avoid the Bragg regime and is efficiently coupled in the subwavelength regime, while the first mode is coupled in the Bragg regime in order to be totally reflected. Within these maps, different taper options can be represented as the lines between the final point of the taper (B) ($w_{bridge}|_{final} = 0\ \mu$m, $\Lambda|_{final} = 355$ nm) and the initial point (A) ($w_{bridge}|_{initial} = 1\ \mu$m, $\Lambda|_{initial}$ to be designed). The pitch at the beginning of the taper $(\Lambda|_{initial})$ should be similar to the final pitch $(\Lambda|_{final})$ to obtain a taper as short as possible. However, the initial pitch has to be sufficiently small to avoid reflections of the second order mode due to proximity to the Bragg regime [see Fig. 2(c)]. An initial pitch of $\Lambda|_{initial} = 250$ nm is chosen as a trade off solution. A taper with linear evolution in pitch and square-root evolution in bridge width is proposed. This configuration maximizes the overlap of the taper path with the reflectivity of the first order mode [see Fig. 2(b)]. The square-root evolution for the bridge width follows the relation

$$w_{bridge}(z) = (w_{bridge}|_{final} - w_{bridge}|_{initial})\sqrt{z} + w_{bridge}|_{initial}. \quad (1)$$

In order to evaluate taper performances, S parameters (transmission, reflection) as a function of the taper length were calculated for back to back configuration [see Fig. 3 (inset)]. We used 50 nm as the final bridge width. Results are shown in Fig. 3. It can be seen that the taper reached the adiabaticity for taper lengths as short as 10 μm. We also notice that only the second order mode is transmitted while the first order mode is completely reflected. This means that compact structures with only the tapers in back to back configuration are enough to obtain

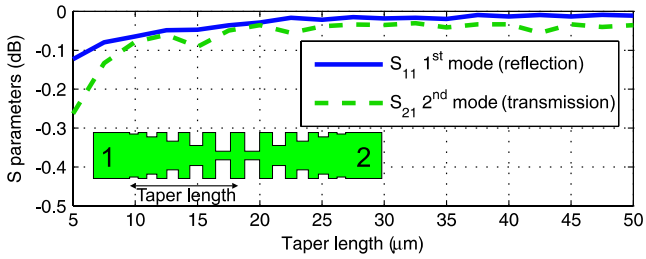

Fig. 3. S parameters of the first- and second-order modes as a function of the taper length. (Inset) Schematic of the structure tested (back to back configuration) (wavelength = 1.55 μm).

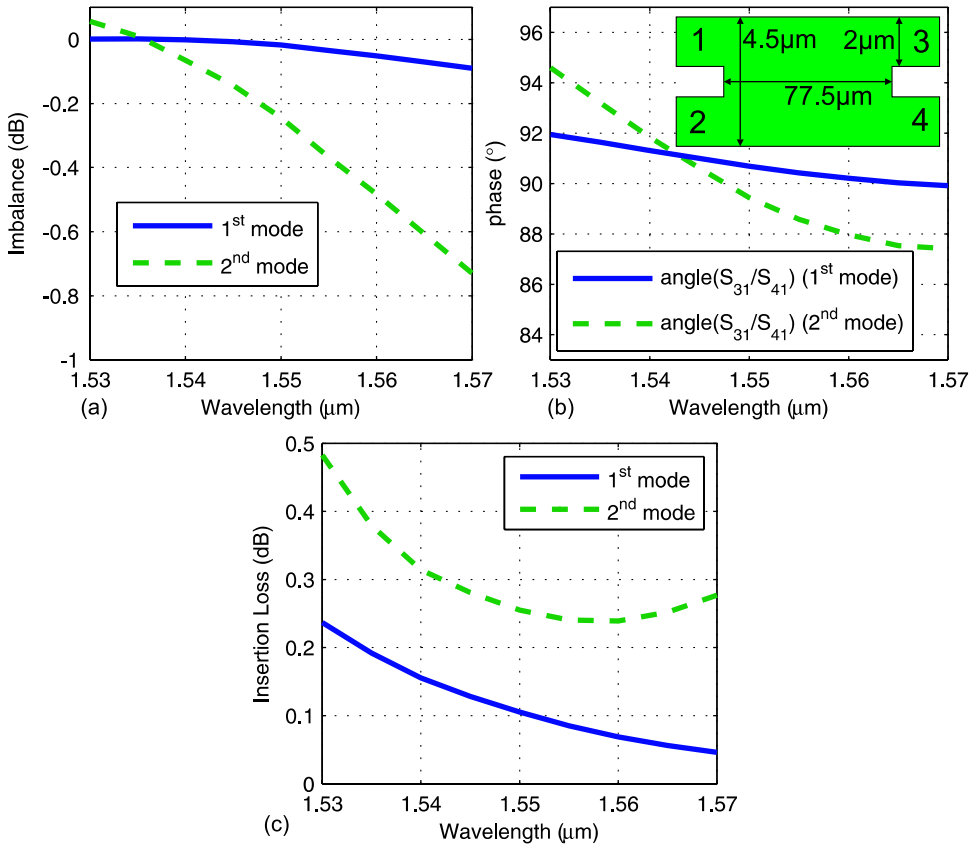

Fig. 4. Performance of the designed MMI. (a) Imbalance (dB). (b) Phase relations between the outputs. (c) Insertion loss, as a function of wavelength. (Inset) Schematic representation of the designed MMI.

the required selectivity between the first- and second-order modes. Two tapers in back to back configuration with a taper length of 30 μm and without periodic waveguide in between are chosen to assure a good performance of the device.

Completing the whole device requires to design the 3 dB/90° couplers working for both the first and the second order modes over a wide bandwidth (C-Band). A MMI coupler, designed using the method proposed in [21], is chosen to implement the 3 dB/90° couplers. The dimensions of the designed MMI [see Fig. 4 (inset)] were 2 μm for the width of input/output waveguides, 500 nm for the gap between the two input and output waveguides, 4.5 μm for the width of the MMI zone, and 77.5 μm for its length. The device was simulated using a 3-D full-vectorial simulator based on the eigenmode expansion method (EME) [22]. In order to evaluate the performance of the designed MMI, S parameters were calculated as a function of the wavelength.

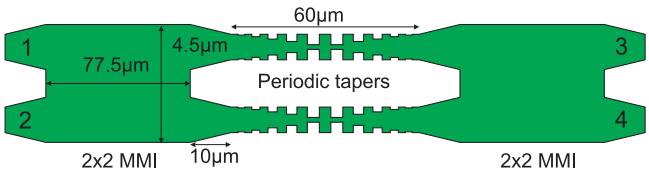

Fig. 5. Layout of the complete device (not to scale).

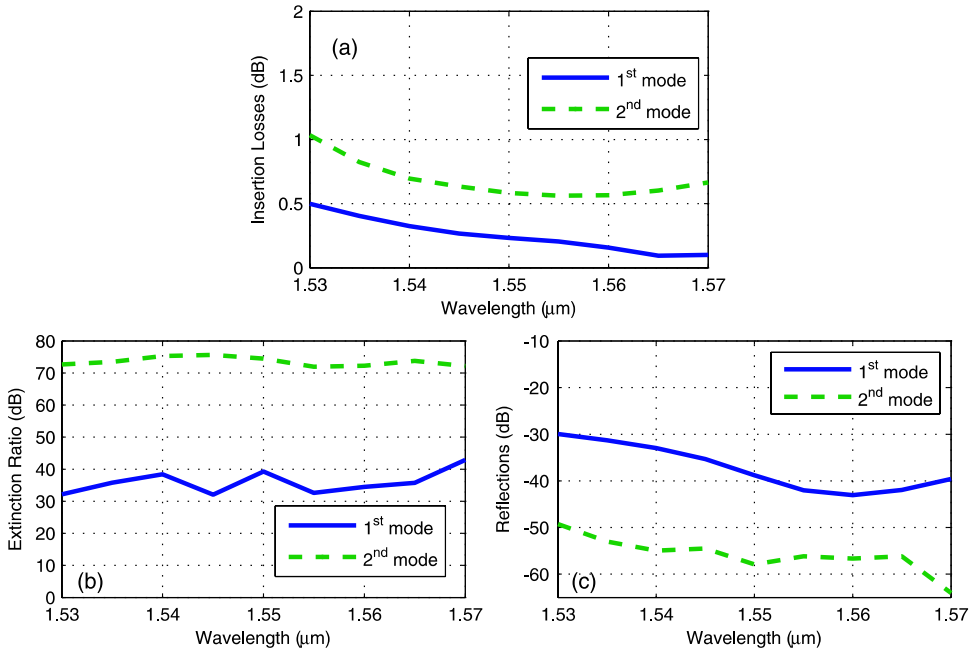

Fig. 6. Performance of the complete device. (a) Insertion Losses. (b) Extinction Ratio. (c) Reflections.

Results are shown in Fig. 4, where Imbalance, phase relation, and Insertion Loss of the MMI are represented. It can be seen that the overall performance is better for the first mode than for the second mode. This behavior can be understood since the decomposition of the second mode into the modes of the MMI zone rely on higher order modes that are less paraxial. However, the Insertion Loss in the C-Band is lower than 0.5 dB for both modes, the Imbalance is below 1 dB and the phase error under 5°.

4. Simulation Results of the Complete Device

Finally, the layout of the complete add/drop mode division multiplexer is shown in Fig. 5. It comprises periodic tapers in back to back configuration and two MMIs, with tapers to adapt the width of the waveguides with the MMI input/output widths.

The simulation of the performance of the complete device is not straightforward using a FDTD simulation tool, due to the length of the input and output MMIs. Then, in order to simulate the complete device in 3-D, S parameters matrices were calculated for each part of the device and then concatenated to obtain the global S parameters of the device. MMI's S parameters were calculated using the 3-D EME method taking into account both the first- and the second-order modes. S parameters of the tapers in back to back configuration are calculated using FDTD [22]. It is necessary to point out that two FDTD simulations are needed to obtain the whole set of S parameters, one for each mode. The resulting S parameters for the complete device are summarized in Fig. 6, where Insertion Losses (IL), Extinction Ratio (ER) and Reflections are represented as a function of wavelength. IL lower than 1 dB in the C-Band was obtained. The

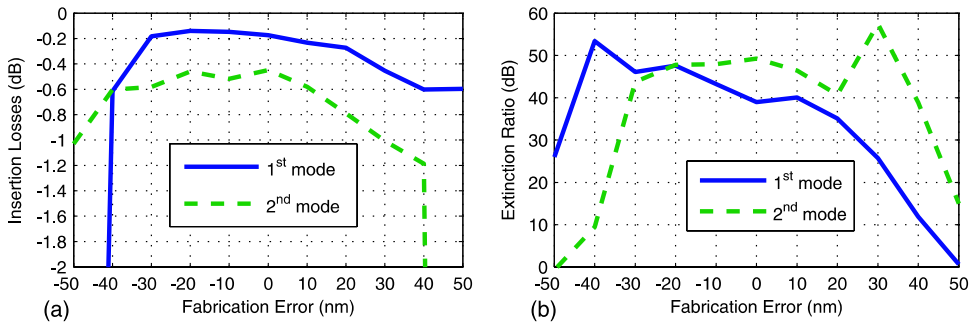

Fig. 7. ER and IL as a function of fabrication error.

device also exhibited low reflections: below –30 dB for both modes. ER parameters for both modes are defined as

$$\mathrm{ER}_{1^{st}\ \mathrm{mode}} = \frac{S_{21}\ 1^{st}\ \mathrm{mode}}{S_{21}\ 2^{nd}\ \mathrm{mode}}$$
$$\mathrm{ER}_{2^{nd}\ \mathrm{mode}} = \frac{S_{41}\ 2^{nd}\ \mathrm{mode}}{S_{41}\ 1^{st}\ \mathrm{mode}} \tag{2}$$

$\mathrm{ER}_{1^{st}\ \mathrm{mode}}$ was limited by the small amount of light from the second mode coupled to port 2, that was mainly due to small reflections of the second mode on the periodic tapers. From Fig. 6(b) it can be seen that ER is higher than 30 dB for the whole C-Band. Light coupled to port 3 coming from the second mode (S_{31} 2nd mode) is below -20 dB. However it can be further reduced by tapering port 3 until achieving single-mode condition in the waveguide. Light coupled to first mode in ports 4 and 3 (S_{41} and S_{31} 1st mode) is below -60 dB, which means that the periodic tapers completely reflect the first mode. Crosstalk is due to mode conversion, i.e., light coupled to the second order mode when we excited with the first order mode and vice versa. The calculated crosstalk between the first and second modes was better than 20 dB in the complete C-Band.

The minimum feature size (MFS) is usually located in the periodic waveguide. The MFS is 50 nm ($w_{bridge}|_{final}$), compatible with 193 nm deep-UV immersion lithography techniques. From Fig. 6, it can be seen that the device is not very wavelength-dependent. This is due to the fact that the working principle in the periodic waveguides exhibits a broadband bandwidth. Furthermore, due to this low wavelength dependency fabrication tolerances are expected to be relatively wide. In order to calculate the fabrication tolerances of the device, IL and ER have been computed as function of the fabrication error. Width changes were considered, it is important to point out that to perform a rigorous tolerance study, the duty cycle was changed accordingly to width variation. In order to lighten the computational effort, a 2-D model was obtained by means of the effective index method (EIM) and simulated using FEXEN [20]. Results are shown in Fig. 7, representing IL and ER as a function of fabrication error. As expected, the device exhibits wide tolerance to fabrication errors exceeding 70 nm (from -35 nm to 35 nm) for IL and ER below than 1 dB and higher than 20 dB, respectively. The state-of-the-art of mode multiplexers in terms of fabrication tolerances is the tapered Asymmetric Directional Coupler (ADC) presented by Dorin *et al.* in [15]. It exhibits 25 nm of fabrication tolerance (from -20 nm to 5 nm) for a coupling loss of 1 dB: less than a half of the fabrication tolerance of our device.

5. Conclusion

In conclusion, a novel kind of Add/Drop Mode Division Multiplexer has been proposed and designed, based on a interferometric structure with periodic waveguides. The device relies on the ability of periodic waveguides to work on the Bragg regime for the first mode and on the SWG

regime for the second one. The design methodology has been presented in detail, as well as device performance. The designed device covers the whole C-Band of optical communications with an IL and ER below 1 dB and higher than 30 dB, respectively. Furthermore, it exhibits wide fabrication tolerances: two times higher than the state-of-the-art.

References

[1] M. J. Paniccia, "A perfect marriage: Optics and silicon," *Optik Photonik*, vol. 6, no. 2, pp. 34–38, May 2011.
[2] A. Shacham, K. Bergman, and L. P. Carloni, "Photonic networks-on-chip for future generations of chip multiprocessors," *IEEE Trans. Comput.*, vol. 57, no. 9, pp. 1246–1260, Sep. 2008.
[3] Y. Kawaguchi and K. Tsutsumi, "Mode multiplexing and demultiplexing devices using multimode interference couplers," *Electron. Lett.*, vol. 38, no. 25, pp. 1701–1702, Dec. 2002.
[4] M. Salsi *et al.,* "Mode-division multiplexing of 2 $\times$ 100 Gb/s channels using an LCOS-based spatial modulator," *J. Lightw. Technol.*, vol. 30, no. 4, pp. 618–623, Feb. 2012.
[5] N. Bai *et al.,* "Mode-division multiplexed transmission with inline few-mode fiber amplifier," *Opt. Exp.*, vol. 20, no. 3, pp. 2668–2680, Jan. 2012.
[6] J. B. Driscoll *et al.,* "Asymmetric Y junctions in silicon waveguides for on-chip mode-division multiplexing," *Opt. Lett.*, vol. 38, no. 11, pp. 1854–1856, Jun. 2013.
[7] W. Chen, P. Wang, and J. Yang, "Mode multi/demultiplexer based on cascaded asymmetric y-junctions," *Opt. Exp.*, vol. 21, no. 21, pp. 25 113–25 119, Oct. 2013.
[8] N. Riesen and J. D. Love, "Design of mode-sorting asymmetric Y-junctions," *Appl. Opt.*, vol. 51, no. 15, pp. 2778–2783, 2012.
[9] Y. Ding *et al.,* "On-chip two-mode division multiplexing using tapered directional coupler-based mode multiplexer and demultiplexer," *Opt. Exp.*, vol. 21, no. 8, pp. 10 376–10 382, Apr. 2013.
[10] J. Wang, S. He, and D. Dai, "On-chip silicon 8-channel hybrid (de) multiplexer enabling simultaneous mode- and polarization-division-multiplexing," *Laser Photon. Rev.*, vol. 8, no. 2, pp. L18–L22, Mar. 2014.
[11] S. Bagheri and W. M. Green, "Silicon-on-insulator mode-selective add–drop unit for on-chip mode-division multiplexing," in *Proc. 6th IEEE Int. Conf. GFP*, 2009, pp. 166–168.
[12] N. Hanzawa *et al.,* "Two-mode PLC-based mode multi/demultiplexer for mode and wavelength division multiplexed transmission," *Opt. Exp.*, vol. 21, no. 22, pp. 25 752–25 760, Nov. 2013.
[13] S. Gross, N. Riesen, J. D. Love, and M. J. Withford, "Three-dimensional ultra-broadband integrated tapered mode multiplexers," *Laser Photon. Rev.*, vol. 8, no. 5, pp. L81–L85, Sep. 2014.
[14] N. Riesen and J. D. Love, "Tapered velocity mode-selective couplers," *J. Lightw. Technol.*, vol. 31, no. 13, pp. 2163–2169, Jul. 2013.
[15] B. A. Dorin and W. N. Ye, "Two-mode division multiplexing in a silicon-on-insulator ring resonator," *Opt. Exp.*, vol. 22, no. 4, pp. 4547–4558, 2014.
[16] L.-W. Luo *et al.,* "WDM-compatible mode-division multiplexing on a silicon chip," *Nat. Commun.*, vol. 5, 2014, Art. ID. 3069.
[17] P. J. Bock *et al.,* "Subwavelength grating periodic structures in silicon-on-insulator: A new type of microphotonic waveguide," *Opt. Exp.*, vol. 18, no. 19, pp. 20 251–20 262, 2010.
[18] R. Halir *et al.,* "Waveguide sub-wavelength structures: A review of principles and applications," *Laser Photon. Rev.*, vol. 9, no. 1, pp. 25–49, Jan. 2015.
[19] D. Pérez-Galacho *et al.,* "Adiabatic transitions for sub-wavelength grating waveguides," in *Proc. ECIO*, 2012, p. 71.
[20] L. Zavargo-Peche, A. Ortega-Monux, J. G. Wanguemert-Perez, and I. Molina-Fernandez, "Fourier based combined techniques to design novel sub-wavelength optical integrated devices," *Progress Electromagn. Res.*, vol. 123, pp. 447–465, 2012.
[21] R. Halir *et al.,* "A design procedure for high-performance, rib-waveguide-based multimode interference couplers in silicon-on-insulator," *J. Lightw. Technol.*, vol. 26, no. 16, pp. 2928–2936, Aug. 2008.
[22] Lumerical Solutions, Inc. [Online]. Available: www.lumerical.com